Am J Nucl Med Mol Imaging 2024;14(4):239-252
www.ajnmmi.us /ISSN:2160-8407/ajnmmi0154301

Original Article

Radiomics-based model for prediction of TGF-β1 expression in head and neck squamous cell carcinoma

Kai Qin[1*], Chen Gong[1*], Yi Cheng[1], Li Li[2], Chengxia Liu[2], Feng Yang[1], Jie Rao[1], Qianxia Li[1]

[1]Department of Oncology, Tongji Hospital, Tongji Medical College, Huazhong University of Science and Technology, Wuhan 430030, Hubei, China; [2]Department of Radiology, Tongji Hospital, Tongji Medical College, Huazhong University of Science and Technology, Wuhan 430030, Hubei, China. [*]Equal contributors.

Received November 7, 2023; Accepted August 8, 2024; Epub August 15, 2024; Published August 30, 2024

Abstract: Objective: To explore the connection between TGF-β1 expression and the survival of patients with head and neck squamous cell carcinoma (HNSCC), as well as whether non-invasive CT-based Radiomics can predict TGF-β1 expression in HNSCC patients. Methods: Data on transcriptional profiling and clinical information were acquired from the TCGA database and subsequently categorized based on the TGF-β1 expression cutoff value. Based on the completeness of enhanced arterial phase CT scans, 139 HNSCC patients were selected. The PyRadiomics package was used to extract radiomic features, and the 3D Slicer software was used for image segmentation. Using the mRMR_RFE and Repeat LASSO algorithms, the optimal features for establishing the corresponding gradient enhancement prediction models were identified. Results: A survival analysis was performed on 483 patients, who were divided into two groups based on the TGF-β1 expression cut-off. The Kaplan-Meier curve indicated that TGF-β1 was a significant independent risk factor that reduced patient survival. To construct gradient enhancement prediction models, we used the mRMR_RFE algorithm and the Repeat_LASSO algorithm to obtain two features (glrlm and ngtdm) and three radiation features (glrlm, first order_10percentile, and gldm). In both the training and validation cohorts, the two established models demonstrated strong predictive potential. Furthermore, there was no statistically significant difference in the calibration curve, DCA diagram, or AUC values between the mRMR_RFE_GBM model and the LASSO_GBM model, suggesting that both models fit well. Conclusion: Based on these findings, TGF-β1 was shown to be significantly associated with a poor prognosis and to be a potential risk factor for HNSCC. Furthermore, by employing the mRMR_RFE_GBM and Repeat_LASSO_GBM models, we were able to effectively predict TGF-β1 expression levels in HNSCC through non-invasive CT-based Radiomics.

Keywords: TCGA, TCIA, head and neck squamous cell carcinoma, Radiomics, TGF-β1 expression, prediction model

Introduction

Head and neck squamous cell carcinoma (HNSCC) is a malignant tumor with a high incidence that develops in the mucous epithelium of the mouth, pharynx, and larynx. The standard treatment for HNSCC is currently a combination of surgery and chemoradiotherapy in clinics; however, patients' survival rates within 5 years are still unsatisfactory, only reaching up to 34% [1-3]. Traditional prognostic indicators of HNSCC, such as clinical stages, p16, human papillomavirus (HPV) status, and Programmed cell death ligand 1 (PD-L1) expression [4], can no longer meet the clinical needs of precision medicine. As a result, more research is required to identify new prognostic indicators for personalized stratified patient care.

Due to the unsatisfactory outcomes of the standard treatment options, immunotherapy has been observed as another therapeutic strategy and has been widely used for the treatment of HNSCC. However, only 15-20% of patients have benefited from this treatment [5], highlighting the need to investigate immune-resistant mechanisms in the immune microenvironment and provide evidence for HNSCC treatment. The transforming growth factor beta (TGF-β) family is a key immunosuppressive gene in HNSCC and is linked to a poor prognosis [6]. TGF-β signal dysfunction promotes tumor progression and metastasis by regulating epithelial cell proliferation, inhibiting cell apoptosis, and inducing genomic instability of tumor cells [7]. PD-L1 is a protein that is crucial to the regulation of the immune system. Similar to TGF-β, PD-L1 is highly expressed in patients with HNSCC. PD-L1 can inhibit lymphocyte activation and induce apoptosis by binding to the PD-1 receptor on lymphocytes' surfaces, allowing tumor cells to escape the immune system. TGF-β promotes tumorigenesis and contributes to drug resistance against PD-L1 monoclonal antibodies. Blocking both PD-L1 and TGF-β signals can enhance a synergistic anti-tumor effect and response rate of PD-1 inhibitors [8]. TGF-β1 is highly expressed in the majority of HNSCCs [9], however, whether it is an independent factor that can predict the survival of HNSCC patients remains unclear.

Radiomics is a high-throughput "image sequencing" that can acquire a large number of image parameters by non-invasive, dynamic, and quantitative detection of tumor features [10]. Radiomics has been regarded as an effective technology in HNSCC for guiding early diagnosis and classification, assessing tumor heterogeneity, and identifying cell constituents in the tumor microenvironment [11]. In addition, radiomics has a high potential for overcoming the limitations of traditional tumor markers [12],

https://doi.org/10.62347/JMKV7596

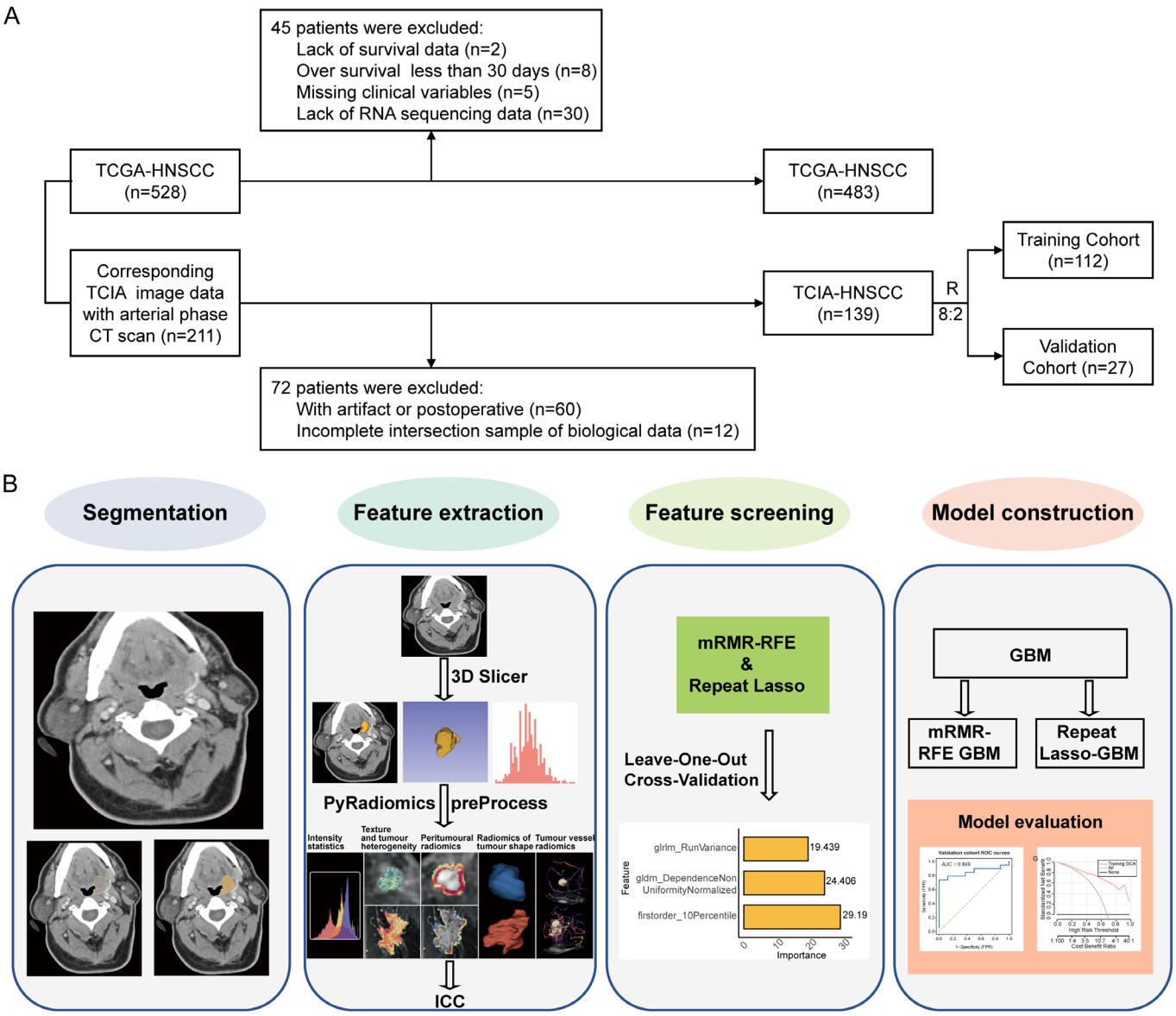

Figure 1. The scheme of patients' selection (A) and radiomics modeling (B). TCGA: The Cancer Genome Atlas, TCIA: The Cancer Imaging Archive, HNSCC: Head and Neck squamous cell carcinoma, ICC: the intraclass correlation coefficient, GBM: Gradient Boosting Machine, mMRM: maximum relevance minimum redundancy, RFE: recursive feature elimination.

because it provides complete three-dimensional information about tumors and allows for non-invasive repetitive analysis using follow-up images. In this study, we used CT-based radiomics to determine the prognostic value of TGF-β1 in HNSCC. We also investigated its potential molecular mechanism and relationship with immune cell constituents using integrated bioinformatics analysis.

Methods

Sources of data & images

Transcriptome profiling data and clinical information of 528 HNSCC patients were collected from the TCGA database (https://portal.gdc.cancer.gov/). About 211 arterial enhanced CT images were obtained from TCIA-HNSC. All data and images are anonymous and public, so they are exempt from ethics and informed consent once approved by the unit ethics committee. TCIA images were used to identify radiomic features and establish models, whereas TCGA data was used for prognosis analysis. Sample selection criteria include preoperative samples, complete clinical data (survival time greater than 30 days), transcriptome sequencing data, arterial phase enhanced CT images, and TCGA-TCIA intersection data. **Figure 1A** shows a brief flow chart.

Analysis of TGF-β1 expression and patients' survival

The R package "survminer" was used to determine the cut-off for TGF-β1 expression. Toil [13] processed RNA sequencing data in FRKM format obtained from UCSC XENA (https://xenaburowser.net/datapages/). The Wil-

coxon test was used to compare TGF-β1 expression in HNSC and normal tissue. Visualization was performed using the R package "ggplot2". TGF-β1 expression in HNSC and normal tissue was compared using the R package "ggplot2". Kaplan-Meier analysis was used to estimate patients' survival rates in the two groups. Univariate and multivariate Cox regression analyses were used to assess the prognostic value of variables such as sex, age, HPV status, nerve invasion, grade, TNM stage, chemoradiotherapy, primary tumor site, and gene expression. The univariate Cox regression method was used to analyze the relationship between TGF-β1 expression and patient prognosis across various subgroups of covariates. The interaction between TGF-β1 and other covariates was analyzed using the likelihood ratio test. In addition, Spearman rank correlation coefficient was used to analyze the correlation between the main variable TGF-β1 and the clinical features of the tumor, and the results were presented using a correlation thermogram. The infiltration of immune cells in TCGA-HNSC patients was assessed using the CIBERSORT (HTTPS://cibersort.stanford.edu/) algorithm to examine the correlation between the infiltration of immune cells and various TGF-β1 expression groups. The Wilcoxon test was applied to analyze the difference in infiltrated immune cells between the high- and low-score groups. The infiltration difference of some functional cells in different score groups was also evaluated with the same method. To predict the gene function and calculate the functional category distribution frequency, Gene Ontology (GO) and enriched Kyoto Encyclopedia of Genes and Genomes (KEGG) pathways were identified using the KOBAS2.0 server (kobas.cbi.pku.edu.cn/). GO (BP, CC, MF) and KEGG enrichment analyses were carried out on the differential genes found in different TGF-β1 expression groups, and the results were illustrated using a bubble diagram. The top 10 significantly enriched pathways were visualized by BP, CC, and MF enrichment analysis, and the top 30 significantly enriched pathways were visualized by KEGG enrichment analysis.

Cohort design, tumor segmentation & radiomic feature determination

The diagrammatic scheme is shown in **Figure 1B**. About 139 images obtained from the TCIA database were grouped randomly (training or validation) according to the ratio of 8:2. Images segmentation was performed by 3D Slicer software (version 4.10.2; https://www.slicer.org/). Before tumor segmentation, the images were preprocessed using the isotropic voxel resampling technique of linear interpolation to achieve the geometric normalization of CT images. All images were visually evaluated independently by an imaging specialist with 10 years of radiology department experience using the double-blind method. Pyradiomics (https://pyradiomics.readthedocs.io/en/latest/index.html) containing 107 features was used for radiomics analysis. Four features in total - texture features, wavelet transform features, volume, and shape features - were obtained. The preProcess function in the R package "caret" was used to standardize the eigenvalues in the training set by z-score. The resulting mean and standard deviation were then used to standardize the characteristic values in the validation set.

Evaluation of consistency

The consistency of the image omics features was evaluated with intraclass correlation efficiency (ICC) based on two doctors' descriptions of VOI [14, 15]. The former described the cases and 20 samples were randomly selected by "random number table". Another radiologist with 8 years of working experience described the cases again and determined radiomics features for consistency evaluation. Generally, ICC ≥ 0.8 is considered as good consistency, 0.51-0.79 is regarded as average consistency, and less than 0.50 is considered poor consistency.

Determination of radiomic features

Over-fitted model with redundant features can affect the result for predicting TGF-β1 expression. Thus, to eliminate redundant features or select optimal features, the maximum correlation-redundancy (mRMR) algorithm and recursive feature elimination (RFE) algorithm were used [16]. Using the maximum correlation minimum redundancy algorithm (or "mRMR" package in the R language), features were first ranked according to their significance. This algorithm maximizes mutual information (MI) with classification labels and minimizes MI with other features. Then, the features that contribute the least to the model were continuously eliminated using the recursive feature elimination (RFE) algorithm, until the necessary number of features remained. Finally, 20 features obtained by the mRMR algorithm and 20 features selected by the RFE algorithm were used for identification of paired and correlated features. Using the R package "caret" and the "gbm" method, the predicted probability scores were ranked using the Gradient Boosting Machine (GBM). Using a set of weak classifiers - typically decision trees - and the cross-validation technique, the GBM algorithm modifies the super-parameters for model establishment. The mRMR_RFE_GBM model was established based on a few radiomic features and the GBM algorithm [17]. The "glmnet" package was used to perform 1000 iterations of Lasso regression on the radiomic features. The top N features with the highest frequency were then chosen as the final subset using the repeat lasso (Least Absolute Shrinkage and Selection Operator) technique [18]. The repeat_LASSO_GBM model in this study was established based on the radiomic features with the top two frequencies and the GBM algorithm.

Evaluation of mRMR_RFE_GBM model and Repeat_LASSO_GBM model

The receiver operating characteristic (ROC) curves, accuracy (ACC), specificity (SPE), sensitivity (sen), positive predictive value (PPV), and negative predictive value (NPV) were used to assess the predictive efficacy of the mRMR_RFE_GBM model and the Repeat_LASSO_GBM model. The Hosmer-Leme show goodness-of-fit test was used to evaluate the calibration curve and determine the degree of calibration of the image omics prediction model. The comprehensive performance of the image ensemble prediction model is determined by the Brier score (measures package). Moreover, the Wilcoxon test was used to compare the TGF-β1 expression predicted by the mRMR_RFE_GBM model and the Repeat_LASSO_GBM model. The area under the curve (AUC) value in the training and validation set was compared using Delong test.

Statistical analysis

SPSS 26.0 software and the R packages (version 4.2.2; http://www.r-project.org/) were used for statistical analysis. The qualitative variables were displayed as numbers (percentages), means ± standard deviations, medians, and interquartile ranges for all the data. The evaluation of gender, age, and other baseline characteristics differing between the training and validation sets was evaluated using independent sample t-tests, Wilcoxon tests, χ^2 tests, chi-square tests, or Fisher's exact tests. Time-to-event data were estimated using the Kaplan-Meier method, and group comparisons were made using the log-rank test. The Cox regression model was used to estimate the HRs and 95% confidence intervals. Risk factor evaluation was assessed with both univariate and multivariate Cox regression analysis.

Results

Clinical features

About 483 HNSCC patients were split into two groups based on the TGF-β1 cut-off (5.208). The clinical information of patients is shown in **Table 1**. There were no significant differences in age, sex, histological grade, TNM staging, and chemoradiotherapy therapy among the two groups (P = 0.847). There were significant differences in HPV status, nerve invasion, and primary tumor location between the two groups.

The correlation analysis of high TGF-β1 expression and poor prognosis

Based on the Toil process transformation analysis, it was found that patients express TGF-β1 at a higher level than normal individuals (**Figure 2A**), with a median expression difference of 1.784 ($P < 0.001$). The correlation between TGF-β1 expression and the survival of patients was analyzed using the Log-Rank test. Kaplan-Meier survival curve showed that the median survival time of patients in the low expression group was 69.43 months, and 46.46 months in the high expression group. These data demonstrated that high TGF-β1 expression was significantly correlated with a poor prognosis ($P < 0.01$) (**Figure 2B**).

The potential prognostic factors were identified using the methods of univariate and multivariate Cox regression. The results of the univariate analysis showed that TGF-β1 was a risk factor for overall survival (HR = 1.876, 95% CI = 1.335-2.635, $P < 0.001$), other hazardous variables include nerve invasion (HR = 2.207, 95% CI 1.552-3.139, $P < 0.001$), T stage (HR = 1.842, 95% CI 1.348-2.516, $P < 0.001$), sex (HR = 0.001, 95% CI 1.362-2.623, $P < 0.001$) and radiotherapy (HR = 0.477, 95% CI 0.36-0.633, $P < 0.001$) (**Table 2**). The results of multivariate analysis showed that TGF-β1 (HR = 1.773, 95% CI = 1.231-2.555, P = 0.002), nerve invasion (HR = 1.676, 95% CI = 1.155-2.433, P = 0.007), N stage (HR = 1.943, 95% CI 1.37-2.755, $P < 0.001$) and radiotherapy (HR = 0.364, 95% CI 0.265-0.501, $P < 0.001$) were all independent risk factors for the overall survival (**Table 2**). The results remained statistically significant even after the most stringent Bonferroni multiple tests were applied to correct it, P = 0.002 < 0.05/15 = 0.0033.

The comparison analysis in high and low TGF-β1 expression groups

According to subgroup analysis, TGF-β1 was a risk factor in cohorts under 60 years old (HR = 1.891, 95% CI = 1.111-3.218, P = 0.019) and older than 60 years old (HR = 1.878, 95% CI = 1.235-2.865, P = 0.003). Furthermore, there was no correlation found between TGF-β1 expression and age (P = 0.97), TGF-β1, various HPV statuses, nerve invasion, and the primary tumor site subgroup. In addition, the correlation between TGF-β1 expression and clinical features was analyzed by the Spearman grade correlation coefficient. The heatmap showed that TGF-β1 was significantly correlated with tumor grade and nerve invasion ($P < 0.01$) (**Figure 2C**). The violin chart demonstrated that the group with high TGF-β1 expression had a significantly decreased number of infiltrated CD8 T cells, naive B cells, and M0 macrophages (P < 0.001) (**Figure 2F**). GO enrichment analysis indicated that genes showing differential expression between high and low TGF-β1 expression were significantly enriched in pathways associated with DNA-binding transcription factor binding, GTP enzyme binding, and transcription auxiliary regulator activity (**Figure 2E**). Similarly, the KEGG enrichment analysis showed that these genes were significantly enriched in the tumor necrosis factor signaling pathway as well as in other cell cycle or apoptotic-related pathways (**Figure 2D**).

The comparison of clinical characteristics and consistency in the HNSCC cohort

There was no difference in the clinical characteristics between the training and validation set ($P > 0.05$) (**Table**

Table 1. Clinical characteristics of HNSC patients in TGF-β1 high and low expression group

Variables	Total (n = 483)	Low (n = 150)	High (n = 333)	*p-value*
Gender, n (%)				0.343
Female	128 (27)	35 (23)	93 (28)	
Male	355 (73)	115 (77)	240 (72)	
Age, n (%)				0.847
~59	211 (44)	67 (45)	144 (43)	
60~	272 (56)	83 (55)	189 (57)	
HPV_status, n (%)				< 0.001
Negative	68 (14)	17 (11)	51 (15)	
Positive	30 (6)	19 (13)	11 (3)	
Unknown	385 (80)	114 (76)	271 (81)	
Perineural_invasion, n (%)				< 0.001
NO	181 (37)	64 (43)	117 (35)	
Unknown	141 (29)	56 (37)	85 (26)	
YES	161 (33)	30 (20)	131 (39)	
Grade, n (%)				0.011
G1/G2	348 (72)	96 (64)	252 (76)	
G3/G4/GX	135 (28)	54 (36)	81 (24)	
T_stage, n (%)				0.328
T1/T2	173 (36)	59 (39)	114 (34)	
T3/T4/TX/Unknown	310 (64)	91 (61)	219 (66)	
N_stage, n (%)				0.476
N0	164 (34)	47 (31)	117 (35)	
N1/N2/N3/NX/Unknown	319 (66)	103 (69)	216 (65)	
M_satge, n (%)				0.257
M0	174 (36)	48 (32)	126 (38)	
M1/MX/Unknown	309 (64)	102 (68)	207 (62)	
Chemotherapy, n (%)				0.251
NO	322 (67)	94 (63)	228 (68)	
YES	161 (33)	56 (37)	105 (32)	
Radiotherapy, n (%)				0.309
NO	234 (48)	67 (45)	167 (50)	
YES	249 (52)	83 (55)	166 (50)	
Primary_tumor_site, n (%)				< 0.001
Larynx	109 (23)	40 (27)	69 (21)	
Oral Cavity	297 (61)	69 (46)	228 (68)	
Oropharynx/Hypopharynx	77 (16)	41 (27)	36 (11)	

HNSCC: Head and Neck squamous cell carcinoma, TGF-β1: The Transforming growth factor-β1, HPV: human papilloma virus.

3). The ICC data showed that there were 96 radiomics features with a value greater than 0.8, and these features accounted for approximately 89.7% of all features, with a median ICC value of 0.926. The radiomics features identified by both methods had ICC values greater than 0.8 (Table S1), indicating good consistency in the HNSCC cohort.

Identification of radiomics features for constructing models

The top 20 features from the mRMR algorithm and the remaining 20 features from the RFE algorithm were analyzed in conjunction to yield three mutual features: original_glrlm_RunVariance, original_first order_10percentile, and original_gldm_dependence_nonuniformity_normalized. The three features used for constructing the mRMR_RFE_GBM model are shown in **Figure 3**. The two optimal features with top frequencies including original_glrlm_RunVariance and original_ngtdm_Complexity were obtained using the repeat LASSO algorithm (**Figure 4**). The two selected features used for constructing the Repeat_LASSO_GBM model are shown in **Figure 5**.

Evaluation of mRMR_RFE_GBM model and Repeat_LASSO_GBM model

We have added the acc, sensitivity, specificity, positive predictive value, negative predictive value, and brierScore of the training set and verification set in the prediction

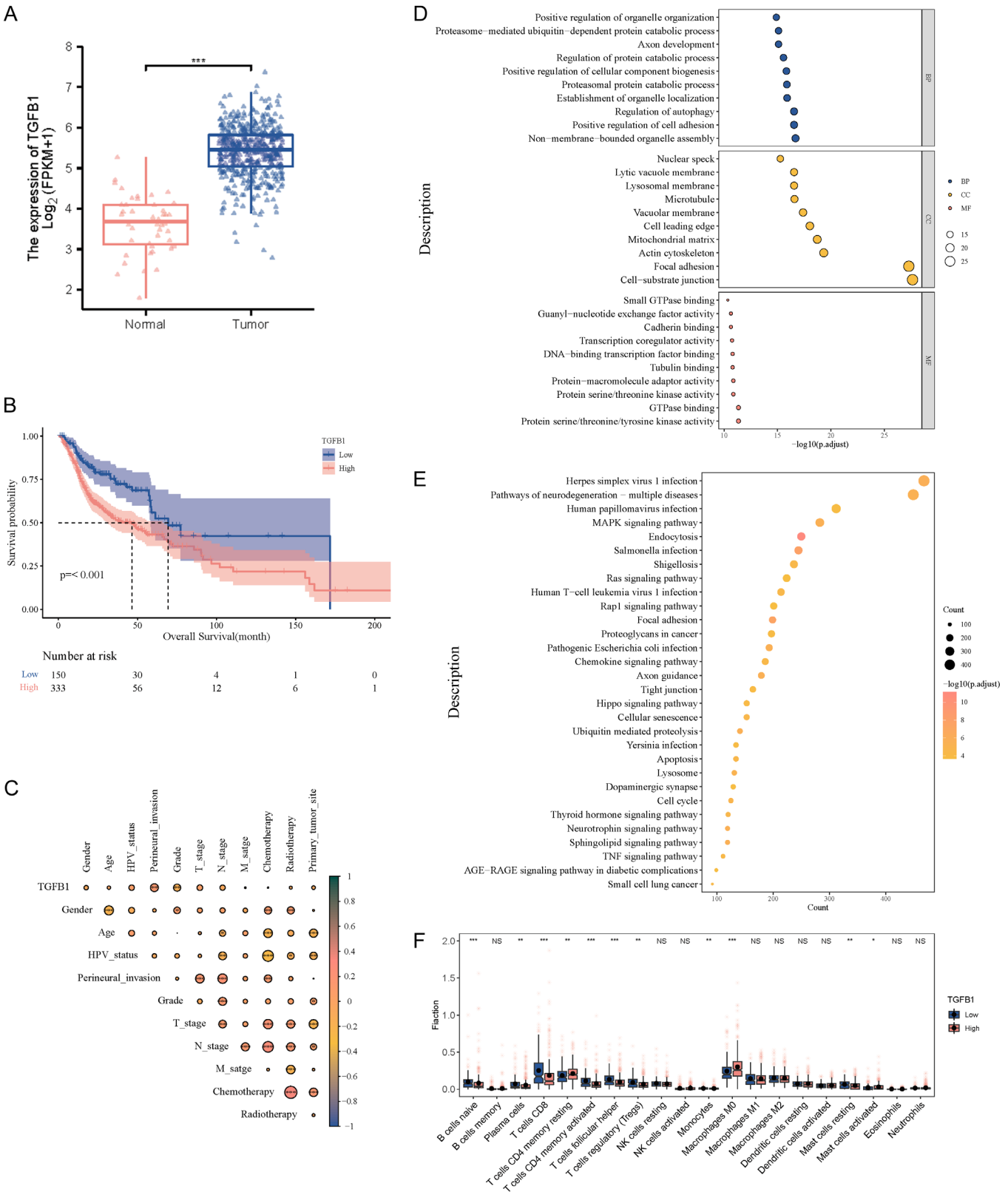

Figure 2. The comparison analysis of high vs. low TGF-β1 expression groups. A: The expression of TGF-β1 in tumor and normal tissues. B: Kaplan-Meier survival analysis. C: Correlation analysis of TGF-β1 and clinical covariates. D: Enrichment analysis of top ten KEGG pathways. E: Enrichment analysis of top thirty GO biological processes. F: Analysis of infiltrated immune cells.

model constructed by mRMR-RFE and Repeat_LASSO in Table S2. The predictive efficacy of the mRMR_RFE_GBM model (**Figure 6**) and Repeat_LASSO_GBM model (Figure S1) were evaluated by the ROC curve. In the training set, the ROC curve showed that the AUC value of the mRMR_RFE_GBM model was 0.911, and the Repeat_LASSO_

Table 2. Univariate and multivariate logistic analysis in TCGA-HNSC

Variable	Univariate analysis		Multivariate analysis	
	HR (95% CI)	*P* value	HR (95% CI)	*P* value
TGFβ1: High vs. Low	1.876 (1.335-2.635)	< 0.001*	1.773 (1.231-2.555)	0.002*
Gender: Male vs. Female	0.737 (0.549-0.989)	0.042*	0.928 (0.673-1.278)	0.646
Age: 60~ vs. ~59	1.262 (0.952-1.674)	0.106	1.197 (0.879-1.631)	0.253
HPV_status: Positive vs. Negative	0.349 (0.105-1.161)	0.086	0.394 (0.111-1.399)	0.15
HPV_status: Unknown vs. Negative	1.117 (0.726-1.717)	0.615	1.13 (0.715-1.786)	0.6
Perineural_invasion: Unknown vs. NO	1.836 (1.263-2.67)	0.001*	1.444 (0.976-2.137)	0.066
Perineural_invasion: YES vs. NO	2.207 (1.552-3.139)	< 0.001*	1.676 (1.155-2.433)	0.007*
Grade: G3/G4/GX vs. G1/G2	0.913 (0.673-1.24)	0.561	0.929 (0.676-1.275)	0.648
T_stage: T3/T4/TX/Unknown vs. T1/T2	1.842 (1.348-2.516)	< 0.001*	2.03 (1.45-2.842)	< 0.001*
N_stage: N1/N2/N3/NX/Unknown vs. N0	1.897 (1.372-2.623)	< 0.001*	1.943 (1.37-2.755)	< 0.001*
M_satge: M1/MX/Unknown vs. M0	1.345 (0.989-1.828)	0.059	0.943 (0.681-1.306)	0.726
Chemotherapy: YES vs. NO	0.989 (0.735-1.33)	0.939	1.208 (0.85-1.717)	0.293
Radiotherapy: YES vs. NO	0.477 (0.36-0.633)	< 0.001*	0.364 (0.265-0.501)	< 0.001*
Primary_tumor_site: Oral Cavity vs. Larynx	1.146 (0.822-1.598)	0.422	1.153 (0.798-1.667)	0.448
Primary_tumor_site: Oropharynx/Hypopharynx vs. Larynx	0.832 (0.504-1.373)	0.471	1.371 (0.779-2.413)	0.274

*reflected the significant difference with the *P* value < 0.05.

GBM model was 0.733. In the validation set, the AUC value of the mRMR_RFE_GBM model was 0.849 and the Repeat_LASSO_GBM model was 0.72. When comparing the two cohorts (training set and validation set), we found that the AUC value of the mRMR_RFE_GBM model in the training set (P = 0.443, P = 0.912) was not statistically different from that in the validation set. Similarly, the AUC value of the Repeat_LASSO_GBM model in the training set (P = 0.443, P = 0.912) was not statistically different from the validation set. These data suggested that the two models fit well. When comparing the two models (mRMR_RFE_GBM model and Repeat_LASSO_GBM model), we observed that the AUC value of the mRMR_RFE_GBM model was significantly higher than the Repeat_LASSO_GBM model in the training cohort (*P* < 0.001), whereas no difference was observed in the validation cohort (P = 0.212). In addition, the calibration curve shows that the predictive result of TGF-β1 expression using a radiomics-based model was consistent with the real value. The DCA diagram demonstrated the strong clinical applicability of the models. Finally, we found that the rad score distribution in the mRMR_RFE_GBM model differed significantly between the training and validation sets, and that the high TGF-β1 expression group displayed a higher rad score (Figure S2C, S2D). The distribution of rad score differed significantly in the training set (*P* < 0.001) of the Repeat_LASSO_GBM model (Figure S2B), but there was no difference in the validation set (*P* > 0.05) between the high and low TGF-β1 expression groups (Figure S2A). In summary, the mRMR_RFE_GBM model and the Repeat_LASSO_GBM model both have great potential in predicting TGF-β1 expression, and the mRMR_RFE_GBM model is relatively better in clinical applicability based on their predictive performance.

Discussion

The two primary factors that decreased the overall median survival time (OS) in patients with advanced HNSCC were high recurrence and metastasis [19]. Therefore, it is imperative to enhance the precancerous diagnosis and prognostic assessment of HNSCC. Previous research has indicated that the expression level of the Combined Positive Score (CPS) and the immunohistochemical p16 status of oropharyngeal squamous cell carcinoma (OPSCC) serve as the diagnostic biomarkers in HNSCC, while tumor mutational burden (TMB) and tumor-infiltrating lymphocytes (TILs) serve as the prognostic biomarkers for immunotherapy [4]. However, there is still a limitation in the ability to detect these documented biomarkers, therefore it is necessary to find novel biomarkers or technologies. Numerous cancer types exhibit elevated expression of TGF-β, which plays a crucial role in several biological processes such as extracellular matrix synthesis, cell growth, and differentiation [20]. These processes ultimately result in tumor progression, invasion, and metastasis [21]. Moreover, KIM et al. [22] identified TGF-β as a marker linked to the prognosis of patients with HNSCC [23-25]. TGF-β1, the most prevalent type in the TGF-β family [21], has been linked to a poor prognosis in several cancers, including HNSCC [21, 26-29]. For instance, there is a significant increase in TGF-β1 expression in the interstitial tissue of HNSCC [9], and the prognosis of HNSCC patients treated with cetuximab is negatively correlated with an elevated TGF-β1 level in plasma [30]. In this investigation, we confirmed that TGF-β1 expression was negatively correlated with patient prognosis (*P* < 0.01) and that it was an independent prognostic marker in HNSCC. TGF-β inhibition has demonstrated great promise in the treatment of tumors in recent years. According to earlier

Table 3. Clinicopathologic features in training and validation groups

Variables	Total (n = 139)	Train (n = 112)	Validation (n = 27)	*p*-value
TGF-β1, n (%)				0.983
Low	44 (32)	36 (32)	8 (30)	
High	95 (68)	76 (68)	19 (70)	
Age, n (%)				0.207
~59	64 (46)	55 (49)	9 (33)	
60~	75 (54)	57 (51)	18 (67)	
Gender, n (%)				0.582
Female	34 (24)	29 (26)	5 (19)	
Male	105 (76)	83 (74)	22 (81)	
HPV_status, n (%)				0.735
Negative	15 (11)	13 (12)	2 (7)	
Positive/Unknown	124 (89)	99 (88)	25 (93)	
Grade, n (%)				0.439
G1/G2	97 (70)	76 (68)	21 (78)	
G3/G4/GX	42 (30)	36 (32)	6 (22)	
T_stage, n (%)				0.759
T1/T2	42 (30)	35 (31)	7 (26)	
T3/T4/TX/Unknown	97 (70)	77 (69)	20 (74)	
N_stage, n (%)				0.996
N0	54 (39)	43 (38)	11 (41)	
N1/N2/N3/NX/Unknown	85 (61)	69 (62)	16 (59)	
M_satge, n (%)				0.77
M0	66 (47)	52 (46)	14 (52)	
M1/MX/Unknown	73 (53)	60 (54)	13 (48)	
Radiotherapy, n (%)				0.464
NO	68 (49)	57 (51)	11 (41)	
YES	71 (51)	55 (49)	16 (59)	
Primary_tumor_site, n (%)				0.061
Larynx	34 (24)	24 (21)	10 (37)	
Oral Cavity	84 (60)	73 (65)	11 (41)	
Oropharynx/Hypopharynx	21 (15)	15 (13)	6 (22)	
Chemotherapy, n (%)				0.945
NO	96 (69)	78 (70)	18 (67)	
YES	43 (31)	34 (30)	9 (33)	
Perineural_invasion, n (%)				0.286
NO	48 (35)	36 (32)	12 (44)	
Unknown	49 (35)	39 (35)	10 (37)	
YES	42 (30)	37 (33)	5 (19)	
OS, n (%)				0.249
Alive	88 (63)	74 (66)	14 (52)	
Dead	51 (37)	38 (34)	13 (48)	
OS time, Median (Q1, Q3)	29.63 (14.42, 49.07)	29.7 (13.51, 48.97)	25.13 (17.87, 49.27)	0.994

TGF-β1: The transforming growth factor-β1, HPV: human papilloma virus, OS: overall survival.

research, tumors that express TGF-β can increase the anti-tumor activity of EGF receptor-targeted therapy. On the other hand, another study shows that TGF-β inhibition can improve the anti-tumor activity of targeted therapy in vivo [31]. Numerous RCT clinical trials are investigating the use of different TGF-β inhibitors in tumors to establish their role in the treatment of cancer. Currently, TGF-β vaccines Lucanix (NCT00676507, NCT02346747) and gemenovatuc (NCT03495921) target antisense oligonucleotides (ASO): AP12009 (NCT00844064, NCT00761280) and ISTH0036 (NCT02406833) and TGF-β inhibitors that are small molecules: Galunisertib (NCT01582269, NCT02160106) and numerous other kinds are under numerous clinical RCT studies. Some of the tri-

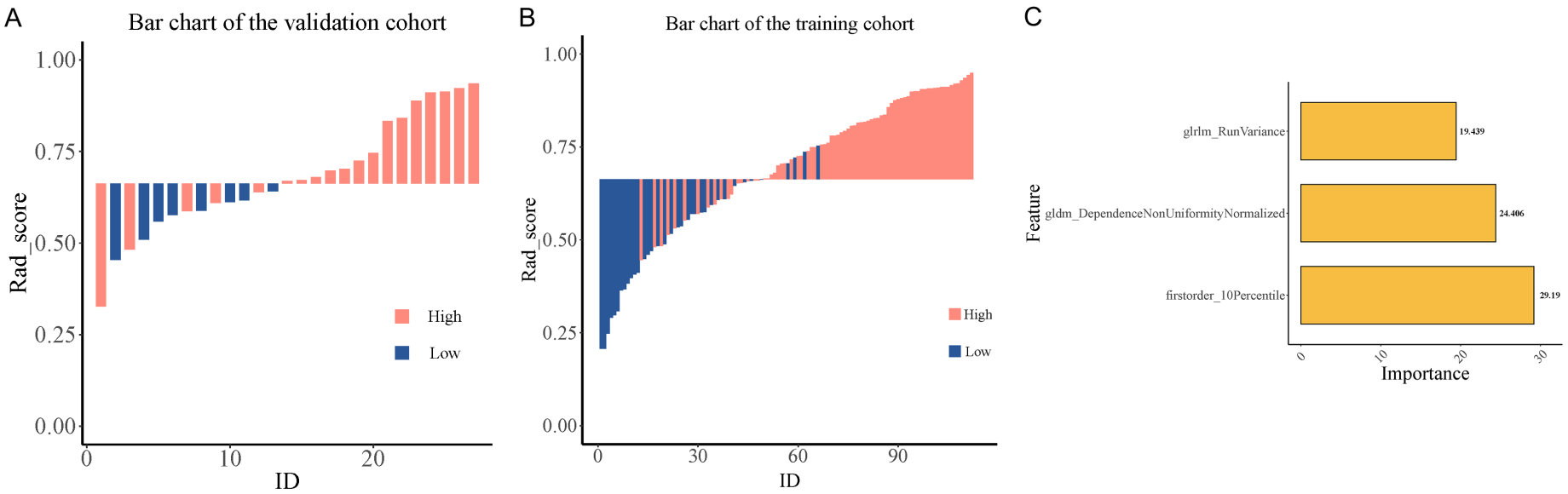

Figure 3. Screening of radiomics features by repeat mRMR_RFE_GBM algorithm. (A, B) Bar chart of training cohort (B) and validation cohort (A). (C) Ranking imaging features based on their predictive potential.

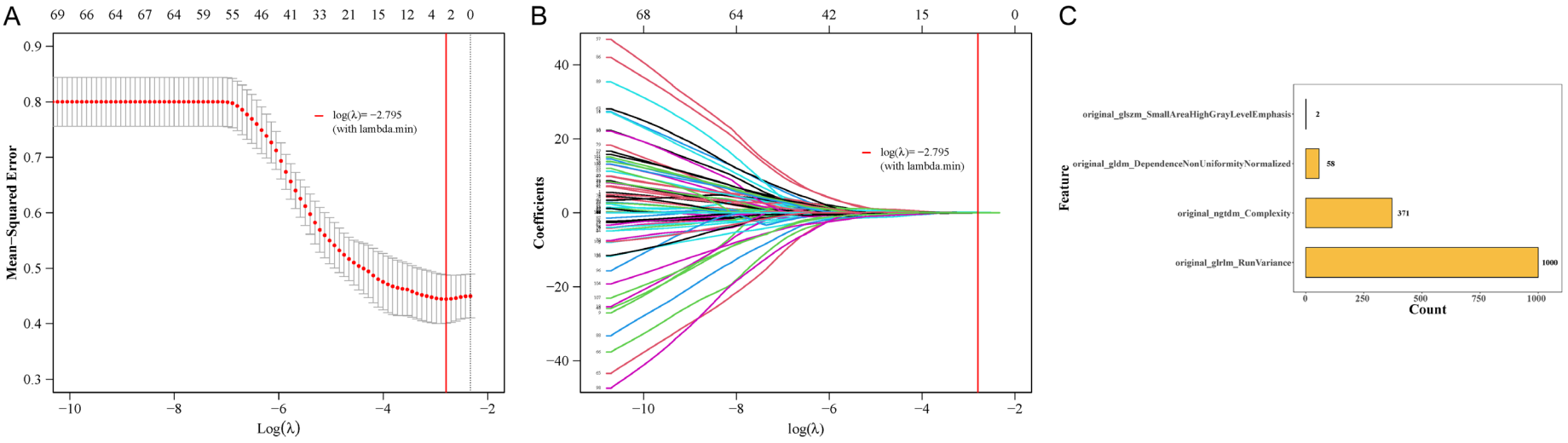

Figure 4. A: Plot of ten-fold cross-validation for determining the optimal lambda (tuning parameter). B: Plot of non-zero coefficients or image features against the L1 norm penalty. C: Four top features based on their frequencies were identified using the method of 1000 lasso regression.

Figure 5. Screening of radiomics features by LASSO-GBM algorithm. (A, B) Bar chart of training cohort (B) and validation cohort (A). (C) Ranking imaging features based on their predictive potential.

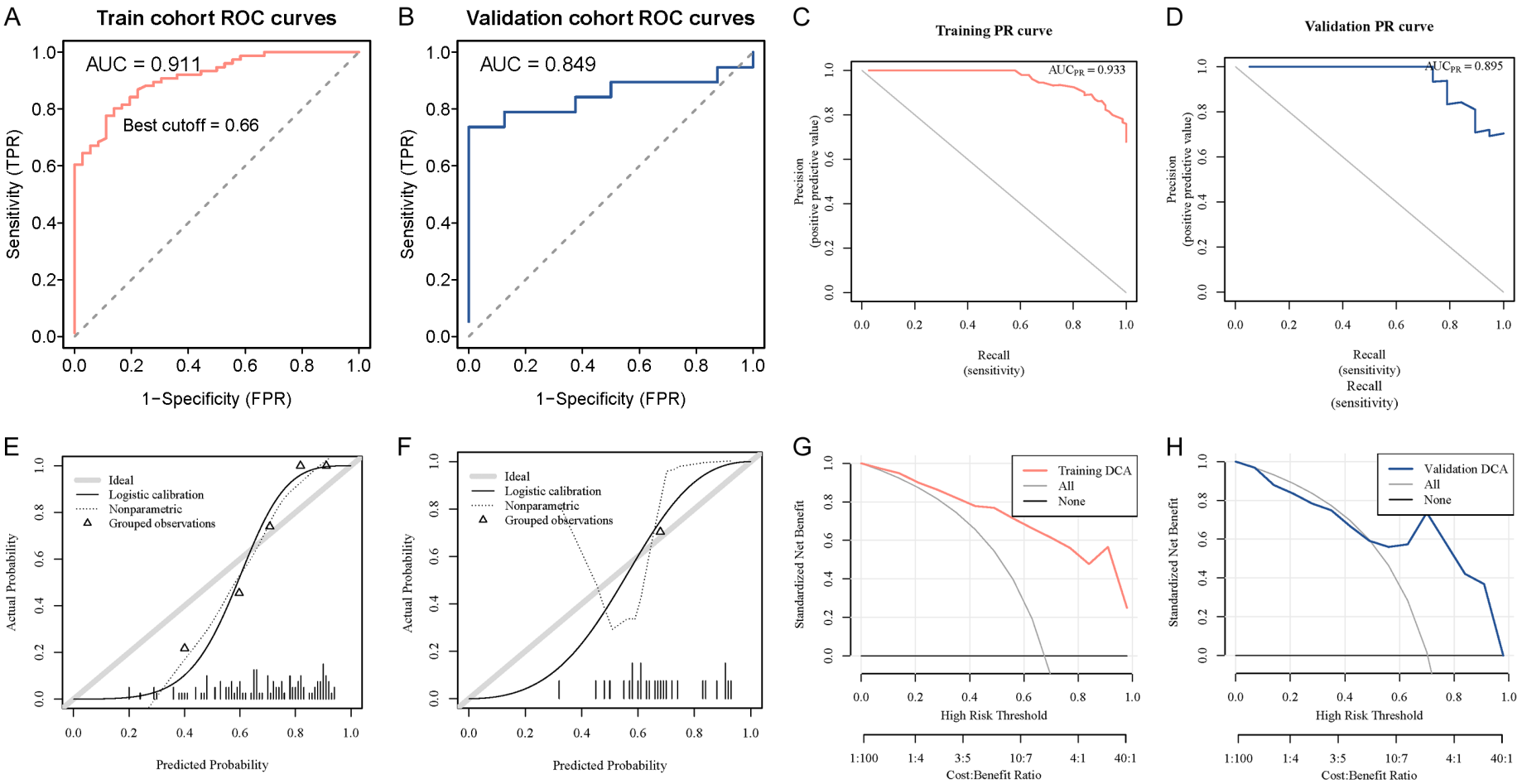

Figure 6. Comprehensive analysis of mRMR_RFE_GBM model for predicting TGF-β1 expression. (A, B) ROC curve of mRMR_RFE_GBM model in training set (A) and validation set (B). (C, D) Recall curve of mRMR_RFE_GBM model in training set (C) and validation set (D). (E, F) Calibration curve of mRMR_RFE_GBM model in (E) training set and (F) validation set. (G, H) Decision curve of the model in (G) training set and (H) validation set. Gray heavy lines: ideal performance; Dotted lines: real performance; Solid lines: corrected performance.

als have progressed to phase III clinical trials, offering excellent potential for clinical application [32]. Unfortunately, current TGF-β detection methods are typically invasive, costly, and dependent on local tumor tissue, which not only fails to accurately reflect the tumor's overall state but also presents challenges for dynamic observation. Consequently, this study builds a noninvasive imaging prediction model of TGF-β based on the tumor as a whole, which can forecast the prognosis of patients. Non-invasive prediction makes it possible to track TGF-β dynamically, gives rise to the ability to forecast TGF-β-related treatment, and can identify patients who may benefit from TGF-β targeted therapy in the future.

Positron emission tomography/computed tomography (PET-CT) [33] or positron emission tomography/magnetic resonance imaging (PET-MR) [34] is a rare imaging modality used in radiomics studies for HNSCC. The most common imaging modality is computed tomography (CT) [35], followed by magnetic resonance imaging (MRI) [36-39]. Gray level co-occurrence matrix (GLCM), gray level run-length matrix (GLRLM), gray level size-area matrix (GLZM), and gray level distance-area matrix (GLDZM) are the features that are most frequently seen [38]. For instance, Francesco Mungai et al. found that a model for predicting human papillomavirus in oropharyngeal squamous cell carcinoma can be created using GLRLM [35]. Wenwu et al. found that GLCM can distinguish the differentiation degree of HNSCC based on CT radiation characteristics [40]. In our study, 20 radiomics features were obtained using the mRMR and RFE algorithms. The optimal feature subset obtained by the mRMR_RFE algorithm included one first-order feature and two second-order features. All the optimal feature subset obtained by the Repeat_LASSO algorithm are second-order features. In all these features, the gray run-length matrix (GLRLM) was the best one for both the mRMR_RFE_GBM model and the Repeat_LASSO_GBM model.

The radiomics studies of HNSCC encompass a wide range of topics, such as prognostic marker identification, molecular subtype classification, pathological feature discrimination, stages and risk stratification, and prediction of anti-tumor therapy side effects [36]. One model that can effectively distinguish the differentiation degree of HNSCC is the random forest classifier model, which is based on CT radiomics features [40]. With the help of a random forest classifier model built using CT radiomics features, Tanzhu et al. predicted the TP53 and HPV mutation status in patients with HNSCC [41]. Dang M et al. used the subset size forward selection algorithm to establish a radiomics model, and the accuracy of this model in predicting p53 status was 81.3% [42]. In Radiomics models currently, feature selection techniques such as mRMR_RFE and Repeat_LASSO, along with other embedding and packaging methods, are frequently employed to lower the risk of overfitting. Numerous high-quality radiomics [43-48] employ the mRMR_RFE and Repeat_LASSO algorithms as feature screening techniques. The purpose of feature screening is to get the best image omics features and build an image omics mode. The radiomics model in this study was constructed using mRMR-RFE and LASSO, the two most popular feature screening techniques. When the models constructed by the two feature screening techniques were compared, it was discovered that the radiomics model created by mRMR-RFE outperformed LASSO (Training AUC: 0.911 vs. 0.733, Validation AUC: 0.849 vs. 0.72). Additionally, the calibration curve demonstrates the good degree of calibration of the mRMR-RFE model, which also has a good prediction effect. The DCA display model has a high degree of clinical applicability and can demonstrate the suitability of the construction model's features as determined by mRMR-RFE screening. Using these features, which include GLRLM, NGTDM, and GLDM, we constructed two GBM models in this study: the mRMR_RFE_GBM model and the Repeat_LASSO_GBM model. Furthermore, we discovered that gradient-enhanced CT imaging features can accurately predict TGF-β1 expression in HNSCC, which is strongly correlated with patient prognosis.

Despite its excellent performance, the non-invasive prediction model based on enhanced CT-based radiomics still has limitations. First of all, the outcome of the prognosis analysis could be impacted by data that is sourced from publicly available datasets because of image quality fluctuations. Second, only one radiomics biomarker - TFA1, KMT2D, NSD1, and CD8+ T cells - was employed for prognosis analysis in this work; additional research is necessary on these and other radiomics biomarkers. Third, the predictive value of MRI sequences and PET-CT images is still unknown, and this study only included 128 enhanced CT images. Consequently, more prognostic biomarkers and a larger sample size are required for the stability of the prognostic model, which is crucial in paving the way for future radiomics research on HNSCC.

In summary, TGF-β1 expression is negatively related to the prognosis of HNSCC patients. Based on the gradient enhancement algorithm, CT radiomics offers an alternative image that can accurately and non-invasively predict TGF-β1 expression in HNSCC. Additionally, the Repeat_LASSO_GBM model and the mRMR_RFE_GBM model both have a lot of potential for predicting TGF-β1 expression, but when comparing their predictive performances, the mRMR_RFE_GBM model performs better.

Acknowledgements

The authors thank 51runse (www.51runse.cn) for the English language editing during the preparation of this manuscript. This work was supported by the National Natural Science Foundation of China (82173311).

Disclosure of conflict of interest

The authors declare that the research was conducted in the absence of any commercial or financial relationships

that could be construed as a potential conflict of interest.

Address correspondence to: Qianxia Li, Department of Oncology, Tongji Hospital, Tongji Medical College, Huazhong University of Science and Technology, Wuhan 430030, Hubei, China. E-mail: liqianx110@163.com

References

[1] Johnson DE, Burtness B, Leemans CR, Lui VWY, Bauman JE and Grandis JR. Head and neck squamous cell carcinoma. Nat Rev Dis Primers 2020; 6: 92.

[2] Bray F, Ferlay J, Soerjomataram I, Siegel RL, Torre LA and Jemal A. Global cancer statistics 2018: GLOBOCAN estimates of incidence and mortality worldwide for 36 cancers in 185 countries. CA Cancer J Clin 2018; 68: 394-424.

[3] Wiegand S, Zimmermann A, Wilhelm T and Werner JA. Survival after distant metastasis in head and neck cancer. Anticancer Res 2015; 35: 5499-5502.

[4] Magnes T, Wagner S, Kiem D, Weiss L, Rinnerthaler G, Greil R and Melchardt T. Prognostic and predictive factors in advanced head and neck squamous cell carcinoma. Int J Mol Sci 2021; 22: 4981.

[5] Lee M, Samstein RM, Valero C, Chan TA and Morris LGT. Tumor mutational burden as a predictive biomarker for checkpoint inhibitor immunotherapy. Hum Vaccin Immunother 2020; 16: 112-115.

[6] Budhwani M, Turrell G, Yu M, Frazer IH, Mehdi AM and Chandra J. Immune-inhibitory gene expression is positively correlated with overall immune activity and predicts increased survival probability of cervical and head and neck cancer patients. Front Mol Biosci 2021; 8: 622643.

[7] White RA, Malkoski SP and Wang XJ. TGFB signaling in head and neck squamous cell carcinoma. Oncogene 2010; 29: 5437-5446.

[8] Bell RB, Gough M, Crittenden M and Young K. Moving beyond the T cell synapse for combination neoadjuvant immunotherapy in head and neck cancer. J Clin Invest 2022; 132: e162733.

[9] Lu SL, Reh D, Li AG, Woods J, Corless CL, Kulesz-Martin M and Wang XJ. Overexpression of transforming growth factor beta1 in head and neck epithelia results in inflammation, angiogenesis, and epithelial hyperproliferation. Cancer Res 2004; 64: 4405-4410.

[10] Rizzo S, Botta F, Raimondi S, Origgi D, Fanciullo C, Morganti AG and Bellomi M. Radiomics: the facts and the challenges of image analysis. Eur Radiol Exp 2018; 2: 36.

[11] Fh T, Cyw C and Eyw C. Radiomics AI prediction for head and neck squamous cell carcinoma (HNSCC) prognosis and recurrence with target volume approach. BJR Open 2021; 3: 20200073.

[12] Katsoulakis E, Yu Y, Apte AP, Leeman JE, Katabi N, Morris L, Deasy JO, Chan TA, Lee NY, Riaz N, Hatzoglou V and Oh JH. Radiomic analysis identifies tumor subtypes associated with distinct molecular and microenvironmental factors in head and neck squamous cell carcinoma. Oral Oncol 2020; 110: 104877.

[13] Vivian J, Rao AA, Nothaft FA, Ketchum C, Armstrong J, Novak A, Pfeil J, Narkizian J, Deran AD, Musselman-Brown A, Schmidt H, Amstutz P, Craft B, Goldman M, Rosenbloom K, Cline M, O'Connor B, Hanna M, Birger C, Kent WJ, Patterson DA, Joseph AD, Zhu J, Zaranek S, Getz G, Haussler D and Paten B. Toil enables reproducible, open source, big biomedical data analyses. Nat Biotechnol 2017; 35: 314-316.

[14] Leijenaar RT, Carvalho S, Velazquez ER, van Elmpt WJ, Parmar C, Hoekstra OS, Hoekstra CJ, Boellaard R, Dekker AL, Gillies RJ, Aerts HJ and Lambin P. Stability of FDG-PET radiomics features: an integrated analysis of test-retest and inter-observer variability. Acta Oncol 2013; 52: 1391-1397.

[15] Ma X, Wei J, Gu D, Zhu Y, Feng B, Liang M, Wang S, Zhao X and Tian J. Preoperative radiomics nomogram for microvascular invasion prediction in hepatocellular carcinoma using contrast-enhanced CT. Eur Radiol 2019; 29: 3595-3605.

[16] Huang Y, Wei L, Hu Y, Shao N, Lin Y, He S, Shi H, Zhang X and Lin Y. Multi-parametric MRI-based radiomics models for predicting molecular subtype and androgen receptor expression in breast cancer. Front Oncol 2021; 11: 706733.

[17] Mirniaharikandehei S, Heidari M, Danala G, Lakshmivarahan S and Zheng B. Applying a random projection algorithm to optimize machine learning model for predicting peritoneal metastasis in gastric cancer patients using CT images. Comput Methods Programs Biomed 2021; 200: 105937.

[18] Shur JD, Doran SJ, Kumar S, Ap Dafydd D, Downey K, O'Connor JPB, Papanikolaou N, Messiou C, Koh DM and Orton MR. Radiomics in oncology: a practical guide. Radiographics 2021; 41: 1717-1732.

[19] Burtness B, Harrington KJ, Greil R, Soulières D, Tahara M, de Castro G Jr, Psyrri A, Basté N, Neupane P, Bratland Å, Fuereder T, Hughes BGM, Mesía R, Ngamphaiboon N, Rordorf T, Wan Ishak WZ, Hong RL, González Mendoza R, Roy A, Zhang Y, Gumuscu B, Cheng JD, Jin F and Rischin D; KEYNOTE-048 Investigators. Pembrolizumab alone or with chemotherapy versus cetuximab with chemotherapy for recurrent or metastatic squamous cell carcinoma of the head and neck (KEYNOTE-048): a randomised, open-label, phase 3 study. Lancet 2019; 394: 1915-1928.

[20] Wang J, Xiang H, Lu Y and Wu T. Role and clinical significance of TGF-β1 and TGF-βR1 in malignant tumors (Review). Int J Mol Med 2021; 47: 55.

[21] Hawinkels LJ, Verspaget HW, van Duijn W, van der Zon JM, Zuidwijk K, Kubben FJ, Verheijen JH, Hommes DW, Lamers CB and Sier CF. Tissue level, activation and cellular localisation of TGF-β1 and association with survival in gastric cancer patients. Br J Cancer 2007; 97: 398-404.

[22] Kim HJ, Ahn D, Park TI and Jeong JY. TGFBI expression predicts the survival of patients with Oropharyngeal squamous cell carcinoma. In Vivo 2020; 34: 3005-3012.

[23] Zheng L, Guan Z and Xue M. TGF-beta signaling pathway-based model to predict the subtype and prognosis of head and neck squamous cell carcinoma. Front Genet 2022; 13: 862860.

[24] He F, Chen Z, Deng W, Zhan T, Huang X, Zheng Y and Yang H. Development and validation of a novel ferroptosis-related gene signature for predicting prognosis and immune microenvironment in head and neck squamous cell carcinoma. Int Immunopharmacol 2021; 98: 107789.

[25] Chen YP, Wang YQ, Lv JW, Li YQ, Chua MLK, Le QT, Lee N, Colevas AD, Seiwert T, Hayes DN, Riaz N, Vermorken JB, O'Sullivan B, He QM, Yang XJ, Tang LL, Mao YP, Sun Y, Liu N and Ma J. Identification and validation of novel microenvironment-based immune molecular subgroups of head

and neck squamous cell carcinoma: implications for immunotherapy. Ann Oncol 2019; 30: 68-75.
[26] Fan DM, Wang XJ, He T, Wang Y, Zhou D, Kong GQ, Jiang T and Zhang MM. High expression of TGF-beta1 in the vaginal incisional margin predicts poor prognosis in patients with stage Ib-IIa cervical squamous cell carcinoma. Mol Biol Rep 2012; 39: 3925-3931.
[27] Peng L, Yuan XQ, Zhang CY, Ye F, Zhou HF, Li WL, Liu ZY, Zhang YQ, Pan X and Li GC. High TGF-beta1 expression predicts poor disease prognosis in hepatocellular carcinoma patients. Oncotarget 2017; 8: 34387-34397.
[28] Reis ST, Pontes-Júnior J, Antunes AA, Sousa-Canavez JM, Abe DK, Cruz JA, Dall'oglio MF, Crippa A, Passerotti CC, Ribeiro-Filho LA, Viana NI, Srougi M and Leite KR. Tgf-β1 expression as a biomarker of poor prognosis in prostate cancer. Clinics (Sao Paulo) 2011; 66: 1143-1147.
[29] Talukdar J, Kataki K, Ali E, Choudhury BN, Baruah MN, Bhattacharyya M, Bhattacharjee S and Medhi S. Altered expression of TGF-β1 and TGF-βR2 in tissue samples compared to blood is associated with food habits and survival in esophageal squamous cell carcinoma. Curr Probl Cancer 2021; 45: 100617.
[30] Gilbert J, Schell MJ, Zhao X, Murphy B, Tanvetyanon T, Leon ME, Neil Hayes D, Haigentz M Jr, Saba N, Nieva J, Bishop J, Sidransky D, Ravi R, Bedi A and Chung CH. A randomized phase II efficacy and correlative studies of cetuximab with or without sorafenib in recurrent and/or metastatic head and neck squamous cell carcinoma. Oral Oncol 2015; 51: 376-382.
[31] Bedi A, Chang X, Noonan K, Pham V, Bedi R, Fertig EJ, Considine M, Califano JA, Borrello I, Chung CH, Sidransky D and Ravi R. Inhibition of TGF-β enhances the in vivo antitumor efficacy of EGF receptor-targeted therapy. Mol Cancer Ther 2012; 11: 2429-2439.
[32] Huang CY, Chung CL, Hu TH, Chen JJ, Liu PF and Chen CL. Recent progress in TGF-β inhibitors for cancer therapy. Biomed Pharmacother 2021; 134: 111046.
[33] Freihat O, Tóth Z, Pintér T, Kedves A, Sipos D, Cselik Z, Lippai N, Repa I and Kovács Á. Pre-treatment PET/MRI based FDG and DWI imaging parameters for predicting HPV status and tumor response to chemoradiotherapy in primary oropharyngeal squamous cell carcinoma (OPSCC). Oral Oncol 2021; 116: 105239.
[34] Connor S, Sit C, Anjari M, Lei M, Guerrero-Urbano T, Szyszko T, Cook G, Bassett P and Goh V. The ability of post-chemoradiotherapy DWI ADCmean and (18)F-FDG SUVmax to predict treatment outcomes in head and neck cancer: impact of human papilloma virus oropharyngeal cancer status. J Cancer Res Clin Oncol 2021; 147: 2323-2336.
[35] Mungai F, Verrone GB, Pietragalla M, Berti V, Addeo G, Desideri I, Bonasera L and Miele V. CT assessment of tumor heterogeneity and the potential for the prediction of human papillomavirus status in oropharyngeal squamous cell carcinoma. Radiol Med 2019; 124: 804-811.
[36] Park YM, Lim JY, Koh YW, Kim SH and Choi EC. Machine learning and magnetic resonance imaging radiomics for predicting human papilloma virus status and prognostic factors in oropharyngeal squamous cell carcinoma. Head Neck 2022; 44: 897-903.
[37] Puram SV, Tirosh I, Parikh AS, Patel AP, Yizhak K, Gillespie S, Rodman C, Luo CL, Mroz EA, Emerick KS, Deschler DG, Varvares MA, Mylvaganam R, Rozenblatt-Rosen O, Rocco JW, Faquin WC, Lin DT, Regev A and Bernstein BE. Single-cell transcriptomic analysis of primary and metastatic tumor ecosystems in head and neck cancer. Cell 2017; 171: 1611-1624, e24.
[38] Bruixola G, Remacha E, Jiménez-Pastor A, Dualde D, Viala A, Montón JV, Ibarrola-Villava M, Alberich-Bayarri Á and Cervantes A. Radiomics and radiogenomics in head and neck squamous cell carcinoma: potential contribution to patient management and challenges. Cancer Treat Rev 2021; 99: 102263.
[39] Bos P, van den Brekel MWM, Gouw ZAR, Al-Mamgani A, Waktola S, Aerts HJWL, Beets-Tan RGH, Castelijns JA and Jasperse B. Clinical variables and magnetic resonance imaging-based radiomics predict human papillomavirus status of oropharyngeal cancer. Head Neck 2021; 43: 485-495.
[40] Wu W, Ye J, Wang Q, Luo J and Xu S. CT-based radiomics signature for the preoperative discrimination between head and neck squamous cell carcinoma grades. Front Oncol 2019; 9: 821.
[41] Zhu Y, Mohamed ASR, Lai SY, Yang S, Kanwar A, Wei L, Kamal M, Sengupta S, Elhalawani H, Skinner H, Mackin DS, Shiao J, Messer J, Wong A, Ding Y, Zhang L, Court L, Ji Y and Fuller CD. Imaging-genomic study of head and neck squamous cell carcinoma: associations between radiomic phenotypes and genomic mechanisms via integration of The Cancer Genome Atlas and The Cancer Imaging Archive. JCO Clin Cancer Inform 2019; 3: 1-9.
[42] Dang M, Lysack JT, Wu T, Matthews TW, Chandarana SP, Brockton NT, Bose P, Bansal G, Cheng H, Mitchell JR and Dort JC. MRI texture analysis predicts p53 status in head and neck squamous cell carcinoma. AJNR Am J Neuroradiol 2015; 36: 166-170.
[43] Zhang L, Shen M, Zhang D, He X, Du Q, Liu N and Huang X. Radiomics nomogram based on dual-sequence MRI for assessing Ki-67 expression in breast cancer. J Magn Reson Imaging 2024; 60: 1203-1212.
[44] Zhao B, Xia C, Xia T, Qiu Y, Zhu L, Cao B, Gao Y, Ge R, Cai W, Ding Z, Yu Q, Lu C, Tang T, Wang Y, Song Y, Long X, Ye J, Lu D and Ju S. Development of a radiomics-based model to predict occult liver metastases of pancreatic ductal adenocarcinoma: a multicenter study. Int J Surg 2024; 110: 740-749.
[45] Zhao YY, Xiong ML, Liu YF, Duan LJ, Chen JL, Xing Z, Lin YS and Chen TH. Magnetic resonance imaging radiomics-based prediction of clinically significant prostate cancer in equivocal PI-RADS 3 lesions in the transitional zone. Front Oncol 2023; 13: 1247682.
[46] Fan X, Xie N, Chen J, Li T, Cao R, Yu H, He M, Wang Z, Wang Y, Liu H, Wang H and Yin X. Multiparametric MRI and machine learning based radiomic models for preoperative prediction of multiple biological characteristics in prostate cancer. Front Oncol 2022; 12: 839621.
[47] Dai H, Lu M, Huang B, Tang M, Pang T, Liao B, Cai H, Huang M, Zhou Y, Chen X, Ding H and Feng ST. Considerable effects of imaging sequences, feature extraction, feature selection, and classifiers on radiomics-based prediction of microvascular invasion in hepatocellular carcinoma using magnetic resonance imaging. Quant Imaging Med Surg 2021; 11: 1836-1853.
[48] Wang J, Chen J, Zhou R, Gao Y and Li J. Machine learning-based multiparametric MRI radiomics for predicting poor responders after neoadjuvant chemoradiotherapy in rectal Cancer patients. BMC Cancer 2022; 22: 420.

Table S1. ICC between training and validation groups

	ICC ≥ 0.8	0.5 ≤ ICC < 0.8	ICC < 0.5	ICC_Mean	ICC_Median
Percentage	0.897	0.047	0.056	0.926	0.989
Number	96	5	6	NA	NA

Table S2. Parameter characteristics of training and verification set in the prediction model constructed by mRMR-RFE and Repeat_LASSO

	TGFB1_cat_RS	Areas under the curve (AUC)	Confidence interval (CI)	Areas under the accuracy (ACC)	Sensitivity	Specificity	Positive predictive value	Negative predictive value	BrierScore
mRMR-RFE	Train	0.911	0.86-0.962	0.812	0.776	0.889	0.937	0.653	0.134
	Test	0.849	0.701-0.997	0.815	0.737	1	1	0.615	0.168
Repeat_LASSO	Train	0.733	0.628-0.838	0.759	0.882	0.5	0.788	0.667	0.192
	Test	0.72	0.523-0.918	0.704	0.895	0.25	0.739	0.5	0.193

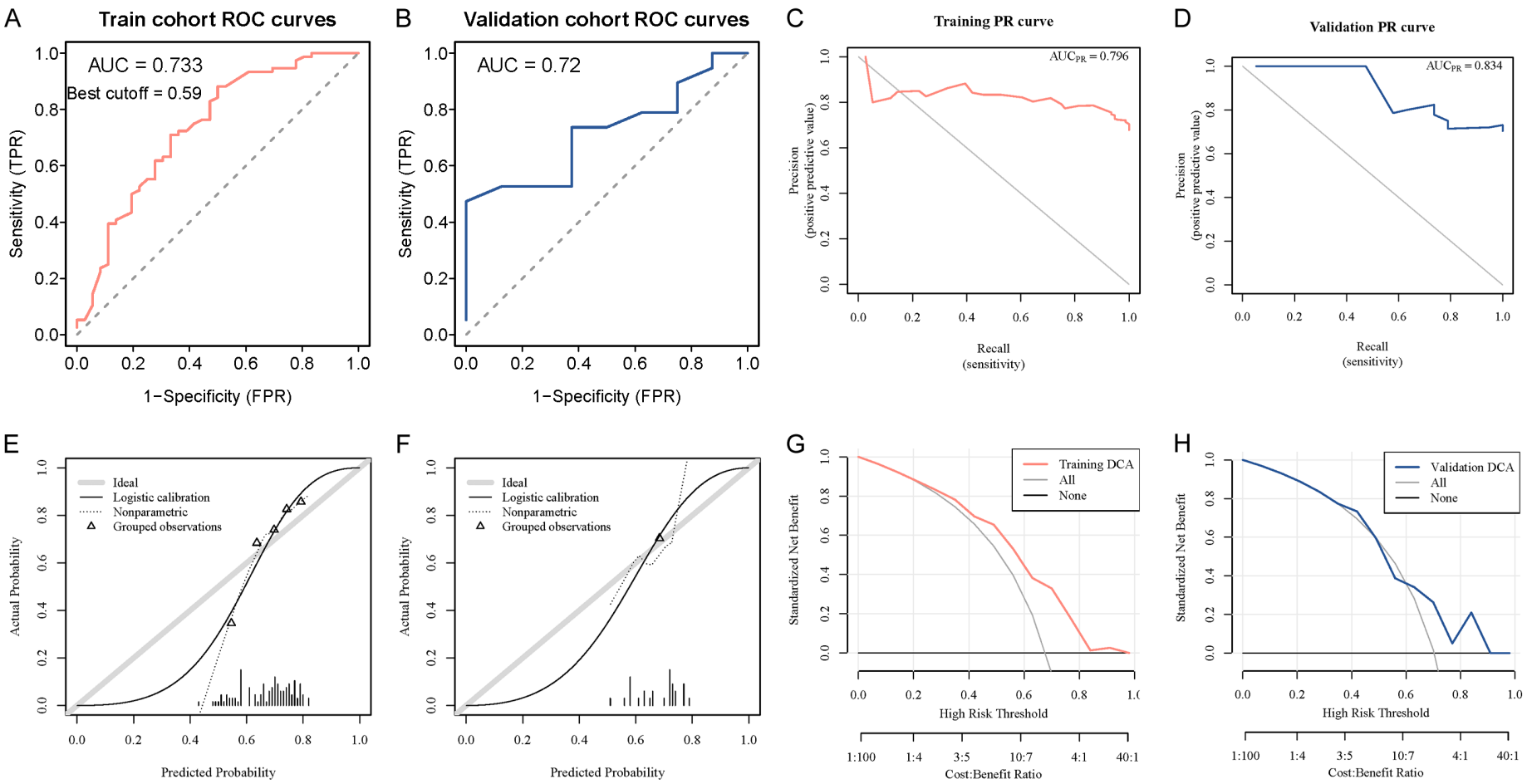

Figure S1. Receiver operating characteristic curves, recall curve, calibration curves and decision curve analysis of the Repeat_LASSO_GBM model for predicting the TGF-β1 expression.

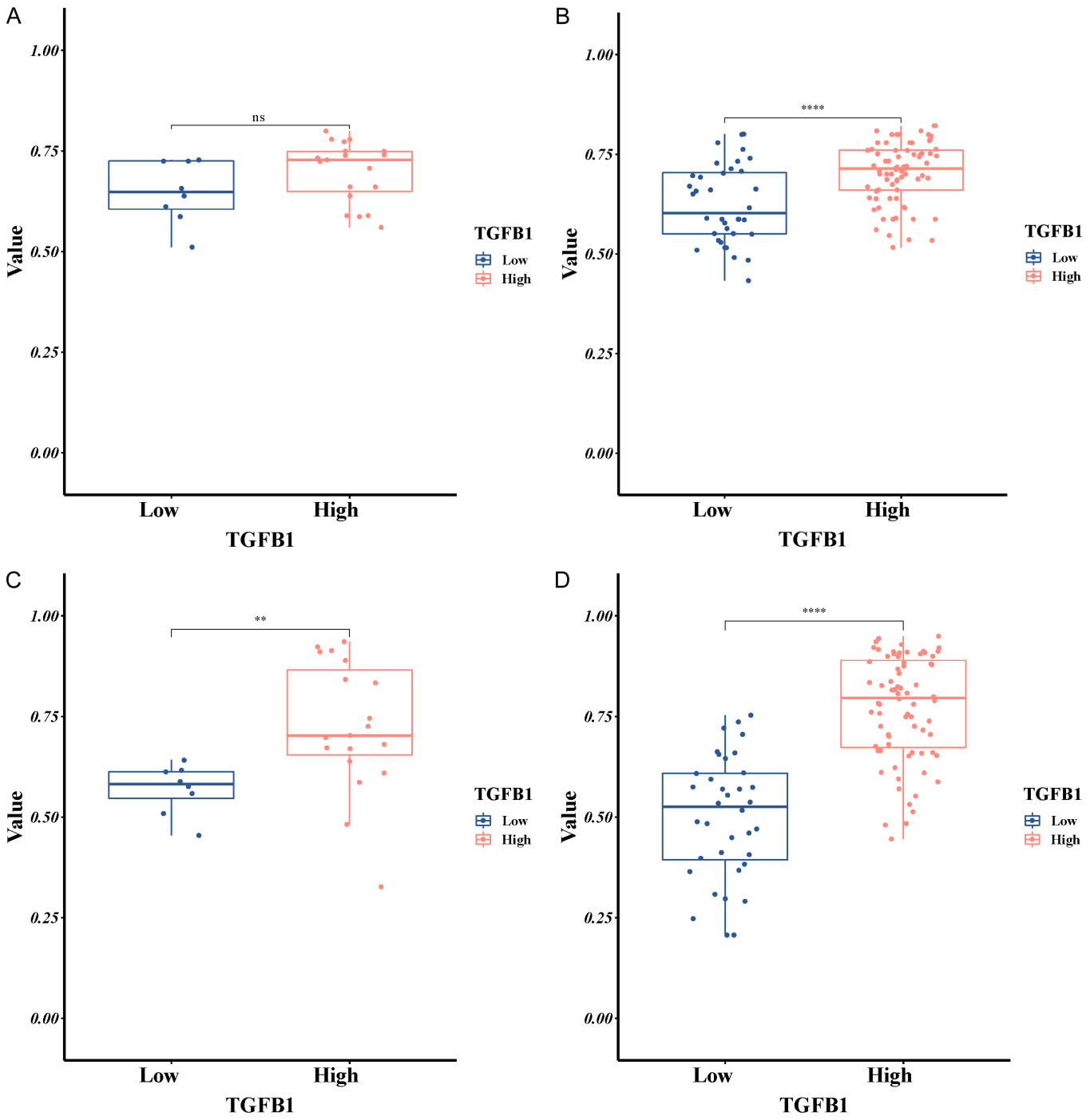

Figure S2. Difference between groups of predicted values of Repeat_LASSO_GBM and mRMR_RFE_GBM models in high and low TGF-β1 expression groups.